Self-doped Ti3+-TiO2 as Photocatalyst for the Reduction of CO2 into Hydrocarbon Fuel under Visible Light Irradiation

ARTICLE *in* NANOSCALE · JULY 2015

Impact Factor: 7.39 · DOI: 10.1039/C5NR02974K

4 AUTHORS, INCLUDING:

Fan Zuo

University of Washington Seattle

38 PUBLICATIONS **1,843** CITATIONS

SEE PROFILE

Pingyun Feng

University of California, Riverside

200 PUBLICATIONS **12,380** CITATIONS

SEE PROFILE

Nanoscale

COMMUNICATION

View Article Online
View Journal | View Issue

Cite this: *Nanoscale*, 2015, **7**, 13369

Received 7th May 2015,
Accepted 1st July 2015

DOI: 10.1039/c5nr02974k

www.rsc.org/nanoscale

Self-doped Ti^{3+}–TiO_2 as a photocatalyst for the reduction of CO_2 into a hydrocarbon fuel under visible light irradiation†

Koroush Sasan,[a] Fan Zuo,[a] Yuan Wang[b] and Pingyun Feng*[a,b]

Self-doped TiO_2 shows visible light photocatalytic activity, while commercial TiO_2 (P25) is only UV responsive. The incorporation of Ti^{3+} into TiO_2 structures narrows the band gap (2.90 eV), leading to significantly increased photocatalytic activity for the reduction of CO_2 into a renewable hydrocarbon fuel (CH_4) in the presence of water vapour under visible light irradiation.

Currently, fossil fuel meets the majority of global energy demands and, at the same time, plays the main role in causing global warming. Carbon dioxide (CO_2) emission from fossil fuels constitutes 84 percent of worldwide greenhouse gas emissions.[1] Regeneration of a fuel from CO_2 by using solar energy is a possible solution to global warming. In fact, the idea of mimicking the overall natural photosynthetic cycle of the chemical conversion of CO_2 into useful fuels has been studied extensively in the last 30 years.[2] Artificial photosynthesis *via* photocatalysts allows the direct conversion of CO_2 and water into valuable hydrocarbons such as CH_4, CH_3OH and C_2H_5OH by using sunlight.[3,4]

Among the present photocatalysts for CO_2 conversion, TiO_2-based semiconductors have been the most popular ones. TiO_2, the first reported photocatalyst, is also one of the most investigated, owing to its nontoxicity, high efficiency, easy availability, and low cost.[5] Many methods, including sol–gel,[6] chemical vapor deposition,[7] solvothermal[8] and microwave[9] methods, have been applied to prepare TiO_2 with various phases and shapes.[10,11] It has been demonstrated that the photocatalytic activity of TiO_2 depends strongly on its phase structure, crystal size, specific surface area, and crystallinity.[12] In spite of extensive studies of CO_2 photoreduction by TiO_2, progress in this area is not as significant as hydrogen photogeneration from water, due to the low efficiency of photocatalysts. The poor photoreduction of CO_2 is caused by several limiting factors such as fast electron–hole recombination rates, low CO_2 affinity to the photocatalyst, and a narrow light absorption wavelength range for wide band-gap semiconductors such as TiO_2.[13] In fact, pure TiO_2 is active under ultraviolet (UV) irradiation that is a very small proportion (about 3–5%) of solar radiation. Therefore, band-gap engineering is required in order to use TiO_2 as efficient catalytic materials. The TiO_2 band gap should be narrow enough to capture part of the visible light spectrum where most of the solar energy exists, and it should also match the CO_2 reduction potential requirements for the desired products.[14]

Doping is one of the popular strategies to overcome the above limitations. The introduction of a metal such as Fe, Mn and Cr or a nonmetal such as N and S in the TiO_2 lattice could create additional energy states within the band gap.[15–17] As a result, the white color of TiO_2 might change, giving a clear sign that visible light has been absorbed. However, the visible light response does not necessarily improve the photocatalytic activity because the introduction of these doping materials may also introduce recombination centres for photogenerated charges.[18] Self-doping could provide a more efficient alternative to the existing doping methods. For instance, a two-dimensional TiO_2 phase with a narrow band gap (*ca.* 2.1 eV) could be formed by the rearrangement of surface atoms of rutile TiO_2.[19] The self-doped TiO_2 (Ti^{3+}–TiO_2) based photocatalytic materials were also reported for H_2 generation and decomposition of gaseous 2-propanol under visible light.[20–22] Recently, we have developed facile one-step combustion and hydrothermal methods to synthesize partially reduced and self-doped TiO_2 (Ti^{3+}–TiO_2), which is a highly active photocatalyst for H_2 generation under visible light.[23] Herein we have demonstrated that these self-doped Ti^{3+}–TiO_2 could be used as visible light photocatalysts for the photoreduction of CO_2 to CH_4. The incorporation of Ti^{3+} into the TiO_2 narrows the band gap (2.90 eV) and extends the light absorption from the UV into the visible range. In addition, the introduction of a Cu^I/Pd on the surface of Ti^{+3}–TiO_2 as a co-catalyst has further enhanced the photocatalytic activity for the conversion of CO_2 to CH_4.

[a]*Department of Chemistry, University of California, Riverside, California 92521, USA. E-mail: pingyun.feng@ucr.edu; Fax: +1 951-827-4713; Tel: +1 951-827-2042*
[b]*Materials Science and Engineering Program, University of California Riverside, CA 92521, USA*

†Electronic supplementary information (ESI) available: Experimental details, XPS, XRD and SEM images. See DOI: 10.1039/c5nr02974k

The rutile TiO_2 with Ti^{3+} self-doping has been synthesized using the hydrothermal method. Briefly, titanium powder and hydrochloric acid were mixed and then transferred to a Teflon-lined stainless-steel autoclave and hydrothermally treated for 12 h at 220 °C. The sample was then washed with distilled water and ethanol several times.[17] The powder X-ray diffraction (XRD) analysis shows that reduced TiO_2 with a rutile phase has formed. A high resolution SEM image reveals that the rutile crystal has a pyramid-shape similar to the Ti^{3+}–TiO_2 previously reported.[17] Electron paramagnetic resonance (EPR) were recorded at low temperature (100 K) to determine the presence of Ti^{3+}. A strong EPR signal was observed at g = 1.97, which can be assigned to a Ti^{3+} peak (Fig. 1c).[23] The Ti^{3+} is formed as a result of reducing Ti^{4+} by H_2, which is produced by a reaction between titanium powder and hydrochloric acid. The Ti^{3+} concentrations were estimated to be ≈4.5 μmol g^{-1}, using numerical double integration of the EPR peak and comparing with a frozen aqueous solution of Cu^{2+}.[24] In addition, X-ray photoelectron spectroscopy (XPS) was used to study the surface elemental composition of the Ti^{3+}–TiO_2 crystal. The XPS result shows the presence of the Ti $2p_{2/3}$ and O 1s peaks. However, the XPS study shows no evidence of Ti^{3+} on the surface of the crystal (Fig. 2a). Having Ti^{3+} in the bulk of the crystal is crucial for the stability of the Ti^{3+}–TiO_2 catalyst since the oxygen defects on the surface are usually not stable enough to survive in the air.[25] Moreover, in comparison with the commercial TiO_2 (P25), our Ti^{3+}–TiO_2 catalyst shows red shifts in the UV/vis absorption spectra, which suggested the narrowing of the band gap from the UV range to the visible light spectrum (Fig. 1d).

Co-catalysts are known to play significant roles in enhancing semiconductors' photocatalytic activity. The incorporation of metals like Pt, Pd, Au, Cu, Ru and Ag on a TiO_2 surface can increase the activity of photoreduction of CO_2 in several ways

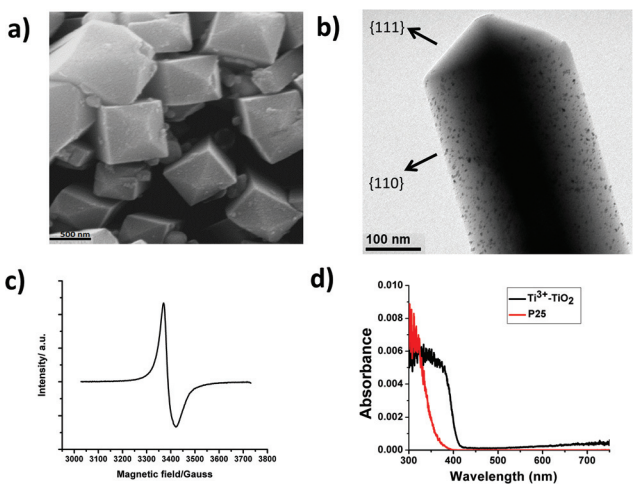

Fig. 1 (a) SEM image of Ti^{3+}–TiO_2. (b) TEM image of a Cu^I/Pd/Ti^{3+}–TiO_2, nanoparticles found on the {111} facets. (c) EPR spectra measured at 100 K. (d) UV/Vis diffuse reflectance spectra for commercial P25 (red) and Ti^{3+}–TiO_2 (black).

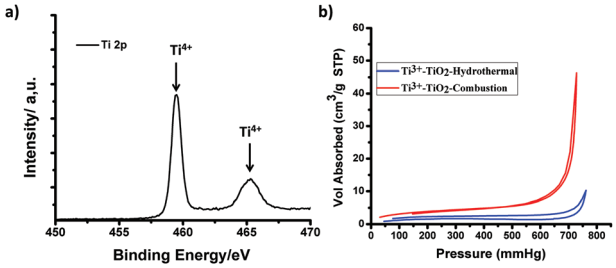

Fig. 2 (a) Ti 2p XPS spectra of Ti^{+3}–TiO_2. No Ti^{3+} signal (at 456.6 eV) was detected. (b) N_2 adsorption–desorption isotherms of Ti^{+3}–TiO_2 from the hydrothermal method and Ti^{+3}–TiO_2 from the combustion method.

such as increasing the charge separation and retarding recombination, trapping of charge carrier, and activating of CO_2 and H_2O.[26] These three factors could thus facilitate further surface transformations, leading to the desired hydrocarbon products. It has also been reported that binary co-catalysts, such as Pt and Au with Cu, can increase the efficiency of the photocatalytic CO_2 reduction, leading mainly to the production of methane with a good selectivity.[27,28] As such, we have introduced both Cu and Pd co-catalysts on the Ti^{3+}–TiO_2. The stepwise photodeposition technique has been used to load Pd and Cu binary co-catalysts on the Ti^{3+}–TiO_2. Briefly in this case, Pd nanoparticles were first introduced onto Ti^{3+}–TiO_2 by photoreducing H_2PdCl_6 in an aqueous suspension. Then, Cu was deposited onto Pd/Ti^{3+}–TiO_2 under UV-vis irradiation for 4 hours using a $CuSO_4$ solution.[27] The chemical states of Pd and Cu in our samples were characterized by XPS analyses. The XPS measurements revealed that the binding energies were 335.1 and 340.2 eV for Pd $3d_{5/2}$ and Pd $3d_{7/2}$, respectively.[29] The Pd/Ti^{+3}–TiO_2 and Cu^I/Pd/ Ti^{3+}–TiO_2 samples confirmed that Pd exists as a metallic state in the samples. The binding energies of Cu $2p_{3/2}$ for the Cu^I/Ti^{+3}–TiO_2 and Pd/Cu^I/Ti^{3+}–TiO_2 samples were about 932.5 eV, which could be contributing to the presence of Cu^I since Cu^0 could be easily oxidized into Cu^I (Cu_2O).[27] Additionally, Fig. 1b shows the high-resolution transmission electron microscopy (HRTEM) image for Cu^I/Pd/Ti^{3+}–TiO_2. The observation of the co-catalysts heavily forming on the {110} facets confirmed that the photogenerated electrons prefer the {110} facets over the {111} facets. The XRD result shows that only Ti^{3+}–TiO_2 diffraction peaks were observed.

The photocatalytic activity of Ti^{3+}–TiO_2-based materials for CO_2 reduction into CH_4 was determined in the gas phase under batch conditions. A Xe lamp (300 W) with a 400 nm cut-on filter was used to cut off the UV light and allow only visible light (>400 nm) to pass through. Fig. 3b shows that the loading of either Pd or Cu^I (existing as Cu_2O) single co-catalysts onto Ti^{3+}–TiO_2 can promote the formation of CH_4. Moreover, the rate of CH_4 formation over the Cu^I/Pd/Ti^{3+}–TiO_2 catalyst was about 6.5 times higher than that over Ti^{3+}–TiO_2 alone. For Pd/Ti^{3+}–TiO_2 and Cu^I/Ti^{3+}–TiO_2 catalysts, the rates of formation were 4.0 and 1.5 times higher, respectively. To prove the photocatalytic CO_2 conversion, control experiments

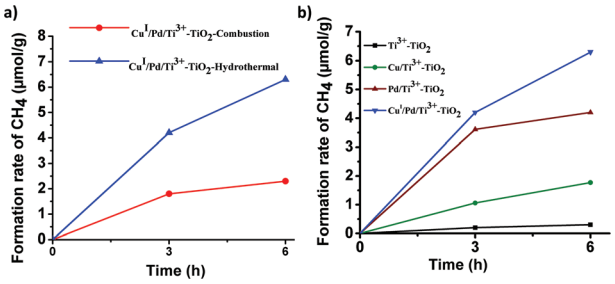

Fig. 3 Time course of evolved CH_4 under visible light (>400 nm) illumination. (a) The CH_4 formation under different photocatalysts, Ti^{3+}–TiO_2 from the combustion method (red) and Ti^{3+}–TiO_2 from the hydrothermal method (blue). (b) The CH_4 formation under different co-catalysts on Ti^{3+}–TiO_2, no co-catalyst (black), Cu^I (green), Pd (brown) and Pd/Cu^I (blue). Reaction conditions: photocatalyst, 0.100 g; visible light (>400 nm), co-catalyst loading ≈1.0% and 1.0 atm water-saturated CO_2.

were conducted, including (I) for long periods in the presence of CO_2 and H_2O with the catalyst in the dark; (II) in the absence of a photocatalyst; and (III) in the absence of CO_2 or H_2O. Analysis of the gas phase in these three controls did not lead to the detection of any reaction products. In addition, we have compared the photoreduction activity of this reported sample prepared by the hydrothermal method with that of the sample prepared by our previously reported combustion method for reduced TiO_2 (Ti^{3+}–TiO_2).[21] The Ti^{3+}–TiO_2 photocatalyst prepared here by the hydrothermal method shows about 2.5 more CH_4 generation than the Ti^{3+}–TiO_2 from combustion.

The photogenerated holes in the valence band oxidize water and generate hydrogen ions through the reaction of $H_2O \rightarrow 2H^+ + \frac{1}{2}O_2 + 2e^-$ (E_0 redox = 0.82 V *vs.* NHE). The photogenerated electrons in the conduction band reduce CO_2 to CH_4 by the reaction of redox $CO_2 + 4H^+ + 8e^- \rightarrow CH_4 + 2H_2O$ (E_0 redox = −0.24 V *vs.* NHE).[30] Functionally, to produce hydrogen cations, the photocatalyst should have the valence band of top energy levels suitable for water oxidation. The bottom energy level of the conduction band should be more negative with respect to the reduction potential of CO_2 into CH_4. The band gaps of Ti^{3+}–TiO_2 were determined to be 2.9 eV using UV-vis absorption spectra. Also, the position of the flat band of Ti^{3+}–TiO_2 was determined using Mott–Schottky plots. The edge of the conduction band was estimated to be −0.45 V (*vs.* NHE), which was more negative than that of E_0 (CO_2/CH_4) (−0.24 *vs.* NHE). Meanwhile, the edge of the valence band was determined to be 2.45 V, which was more positive than that of E_0 (H_2O/H^+) (0.82 V *vs.* NHE). These results indicate that the photogenerated electrons and holes on irradiated Ti^{3+}–TiO_2 can react with the absorbed CO_2 and H_2O to generate CH_4.

Fig. 3 shows the rate formation of CH_4 over the Ti^{3+}–TiO_2 prepared from the hydrothermal and combustion methods under light above 400 nm. The surface areas of the Ti^{3+}–TiO_2 prepared by hydrothermal and combustion methods were determined to be 5.0 $m^2\ g^{-1}$ and 12.3 $m^2\ g^{-1}$, respectively (Fig. 2b), which may seem counterintuitive in contrast to their photo-activity because the Ti^{3+}–TiO_2 prepared from the hydrothermal method shows approximately 2.5 times higher CH_4 formation than the sample prepared from the combustion method. This result indicates that the higher activity of the Ti^{3+}–TiO_2 must come from other structural features such as morphology and crystal shape. In fact, it has been reported that the {111} and {110} facets are prone to collect holes and electrons, which respectively improves the separation of holes and electrons (Fig. 1b).[31,32] Therefore, the higher photocatalytic activity of the Ti^{3+}–TiO_2 might be due to the trapped electrons and holes in different crystal facets of Ti^{3+}–TiO_2, such as the {111} and {110}.[23,33,34] The trapped electrons and holes could suppress rapid recombination that can increase the opportunities to initiate surface reactions, thus enhancing the photocatalytic activity. Moreover, additional evidence suggests that doping the metals as co-catalysts can further enhance electron–hole separation, leading to higher catalytic activity. Our present work further clarified that the formation of CH_4 was also enhanced by loading Pd or Cu^I onto Ti^{3+}–TiO_2, and such an enhancement was much more significant in the case of Cu^I/Pd co-catalysts (Fig. 3b). These results show that the rate of formation of CH_4 over Pd/Ti^{3+}–TiO_2 is higher than Cu^I/Ti^{3+}–TiO_2. The lower photocatalytic activity of Cu^I/Ti^{3+}–TiO_2 might be the result of lower efficiency of separation of photogenerated electron–hole pairs in the Cu^I/Ti^{3+}–TiO_2 catalyst. On the other hand, the Cu^I/Pd/Ti^{3+}–TiO_2 catalyst containing the Pd/Cu^I demonstrated a significantly enhanced activity for the formation of CH_4. The presence of Cu^I in the Cu^I/Pd/Ti^{3+}–TiO_2 structure may cause higher activity by preferential activation and conversion of CO_2 molecules in the presence of H_2O, while the Pd particles effectively extracted the photogenerated electrons from Ti^{3+}–TiO_2.[27,28]

In conclusion, we have studied the photoreduction of CO_2 with a partially reduced non-stoichiometric rutile TiO_2 prepared from the hydrothermal method with active facets. This highly stable photocatalytic material shows a greatly improved efficiency to reduce CO_2 under visible light when compared to the Ti^{3+}–TiO_2 prepared from the combustion method. Additionally, our results demonstrated that using co-catalysts such as Cu^I/Pd might be a potential breakthrough in further improving the photocatalytic activity for CO_2 reduction with H_2O.

Conflict of interest

The authors declare no competing financial interest.

Acknowledgements

This research was supported by the National Science Foundation (CHE-1213795, P.F.).

Notes and references

1 R. K. de_Richter, T. Ming and S. Caillol, *Renewable Sustainable Energy Rev.*, 2013, **19**, 82–106.

2 Z. Goren, I. Willner, A. J. Nelson and A. J. Frank, *J. Phys. Chem.*, 1990, **94**, 3784–3790.
3 H. Sun and S. Wang, *Energy Fuels*, 2013, **28**, 22–36.
4 W. Tu, Y. Zhou and Z. Zou, *Adv. Mater.*, 2014, **26**, 4607–4626.
5 A. Fujishima and K. Honda, *Nature*, 1972, **238**, 37–38.
6 A. Hernández-Gordillo, A. Hernández-Arana, A. Campero and L. I. Vera-Robles, *Langmuir*, 2014, **30**, 4084–4093.
7 A. E. Reeder, S. Agnoli, G. A. Rizzi and G. Granozzi, *J. Phys. Chem. C*, 2014, **118**, 8026–8033.
8 B. P. Bastakoti, Y. Sakka, K. C. W. Wu and Y. Yamauchi, *J. Nanosci. Nanotechnol.*, 2015, **15**, 4747–4751.
9 K. Ullah, Z. Lei, S. Ye, A. Ali and W.-C. Oh, *RSC Adv.*, 2015, **5**, 18841–18849.
10 Y. Jiang, W.-N. Wang, P. Biswas and J. D. Fortner, *ACS Appl. Mater. Interfaces*, 2014, **6**, 11766–11774.
11 J. Fan, L. Zhao, J. Yu and G. Liu, *Nanoscale*, 2012, **4**, 6597–6603.
12 C.-T. Yang, B. C. Wood, V. R. Bhethanabotla and B. Joseph, *J. Phys. Chem. C*, 2014, **118**, 26236–26248.
13 M. Tahir and N. S. Amin, *Appl. Catal., B*, 2015, **162**, 98–109.
14 L. Zhang, Y. Song, J. Feng, T. Fang, Y. Zhong, Z. Li and Z. Zou, *Int. J. Hydrogen Energy*, 2014, **39**, 7697–7704.
15 C. L. Muhich, J. Y. Westcott, T. Fuerst, A. W. Weimer and C. B. Musgrave, *J. Phys. Chem. C*, 2014, **118**, 27415–27427.
16 N. Roy, Y. Sohn, K. T. Leung and D. Pradhan, *J. Phys. Chem. C*, 2014, **118**, 29499–29506.
17 W. Q. Fang, X. L. Wang, H. Zhang, Y. Jia, Z. Huo, Z. Li, H. Zhao, H. G. Yang and X. Yao, *J. Mater. Chem. A*, 2014, **2**, 3513–3520.
18 R. Asahi, T. Morikawa, T. Ohwaki, K. Aoki and Y. Taga, *Science*, 2001, **293**, 269–271.
19 J. Tao, T. Luttrell and M. Batzill, *Nat. Chem.*, 2011, **3**, 296–300.
20 M. Liu, X. Qiu, M. Miyauchi and K. Hashimoto, *Chem. Mater.*, 2011, **23**, 5282–5286.
21 F. Zuo, L. Wang, T. Wu, Z. Zhang, D. Borchardt and P. Feng, *J. Am. Chem. Soc.*, 2010, **132**, 11856–11857.
22 X. Zou, J. Liu, J. Su, F. Zuo, J. Chen and P. Feng, *Chem. – Eur. J.*, 2013, **19**, 2866–2873.
23 F. Zuo, K. Bozhilov, R. J. Dillon, L. Wang, P. Smith, X. Zhao, C. Bardeen and P. Feng, *Angew. Chem., Int. Ed.*, 2012, **51**, 6223–6226.
24 R. F. Howe and M. Gratzel, *J. Phys. Chem.*, 1985, **89**, 4495–4499.
25 P. C. Ricci, A. Casu, M. Salis, R. Corpino and A. Anedda, *J. Phys. Chem. C*, 2010, **114**, 14441–14445.
26 Y. Qu and X. Duan, *Chem. Soc. Rev.*, 2013, **42**, 2568–2580.
27 Q. Zhai, S. Xie, W. Fan, Q. Zhang, Y. Wang, W. Deng and Y. Wang, *Angew. Chem., Int. Ed.*, 2013, **125**, 5888–5891.
28 Ș. Neațu, J. A. Maciá-Agulló, P. Concepción and H. Garcia, *J. Am. Chem. Soc.*, 2014, **136**, 15969–15976.
29 D. Zemlyanov, B. Aszalos-Kiss, E. Kleimenov, D. Teschner, S. Zafeiratos, M. Hävecker, A. Knop-Gericke, R. Schlögl, H. Gabasch, W. Unterberger, K. Hayek and B. Klötzer, *Surf. Sci.*, 2006, **600**, 983–994.
30 Q. Liu, Y. Zhou, J. Kou, X. Chen, Z. Tian, J. Gao, S. Yan and Z. Zou, *J. Am. Chem. Soc.*, 2010, **132**, 14385–14387.
31 T. Ohno, K. Sarukawa and M. Matsumura, *New J. Chem.*, 2002, **26**, 1167–1170.
32 E. Bae, N. Murakami and T. Ohno, *J. Mol. Catal. A: Chem.*, 2009, **300**, 72–79.
33 J. Wang, F. Teng, M. Chen, J. Xu, Y. Song and X. Zhou, *CrystEngComm*, 2013, **15**, 39–42.
34 M.-Y. Xing, B.-X. Yang, H. Yu, B.-Z. Tian, S. Bagwasi, J.-L. Zhang and X.-Q. Gong, *J. Phys. Chem. Lett.*, 2013, **4**, 3910–3917.

